Science Signaling
AAAS

www.sciencesignaling.org/cgi/content/full/11/533/eaar1976/DC1

Supplementary Materials for

Lgl reduces endosomal vesicle acidification and Notch signaling by promoting the interaction between Vap33 and the V-ATPase complex

Marta Portela, Liu Yang, Sayantanee Paul, Xia Li, Alexey Veraksa, Linda M. Parsons, Helena E. Richardson*

*Corresponding author. Email: h.richardson@latrobe.edu.au

Published 5 June 2018, *Sci. Signal.* **11**, eaar1976 (2018)
DOI: 10.1126/scisignal.aar1976

The PDF file includes:

Other Supplementary Material for this manuscript includes the following:
(available at www.sciencesignaling.org/cgi/content/full/11/533/eaar1976/DC1)

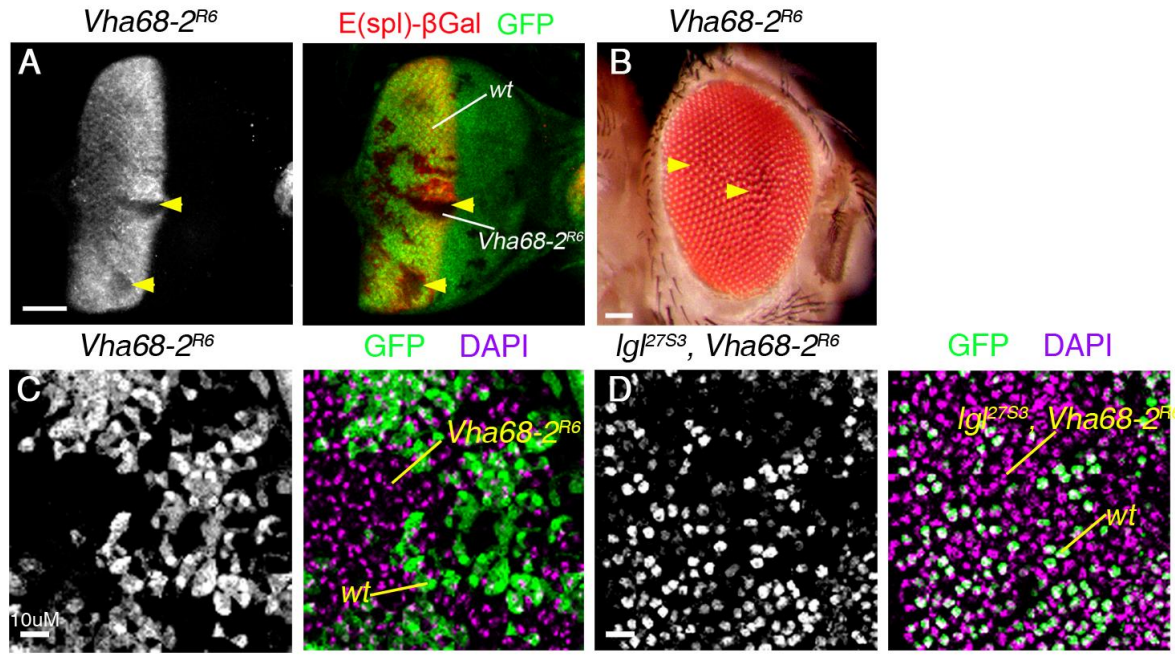

Fig. S1. *Vha68-2* mutant clones show reduced Notch reporter expression, and *lgl Vha68-2* mutant tissue is retained in pupal retinas.

(**A**) *Vha68-2*^{R6} mosaic disc from *E(spl)lacZ* reporter fly stained for β-galactosidase (βGal) Mutant tissue is GFP-negative (arrowheads). (**B**) *Vha68-2*^{R6} mosaic adult female eye. (**C**) Mosaic *Vha68-2*^{R6} pupal eye disc (~52h APF) confocal section revealing the contribution of wild-type (WT) versus mutant tissue in the adult eye. WT clones are GFP-positive, and mutant clones are GFP-negative. Nuclei are marked with DAPI (magenta). (**D**) Mosaic *lgl*^{27S3} *Vha68-2*^{R6} pupal eye disc ~52h APF. For (A-D) N = 2 independent experiments, n = 4 samples analysed per genotype per experiment. Scale bar, 50 μm (A, B) and 10 μm (C, D).

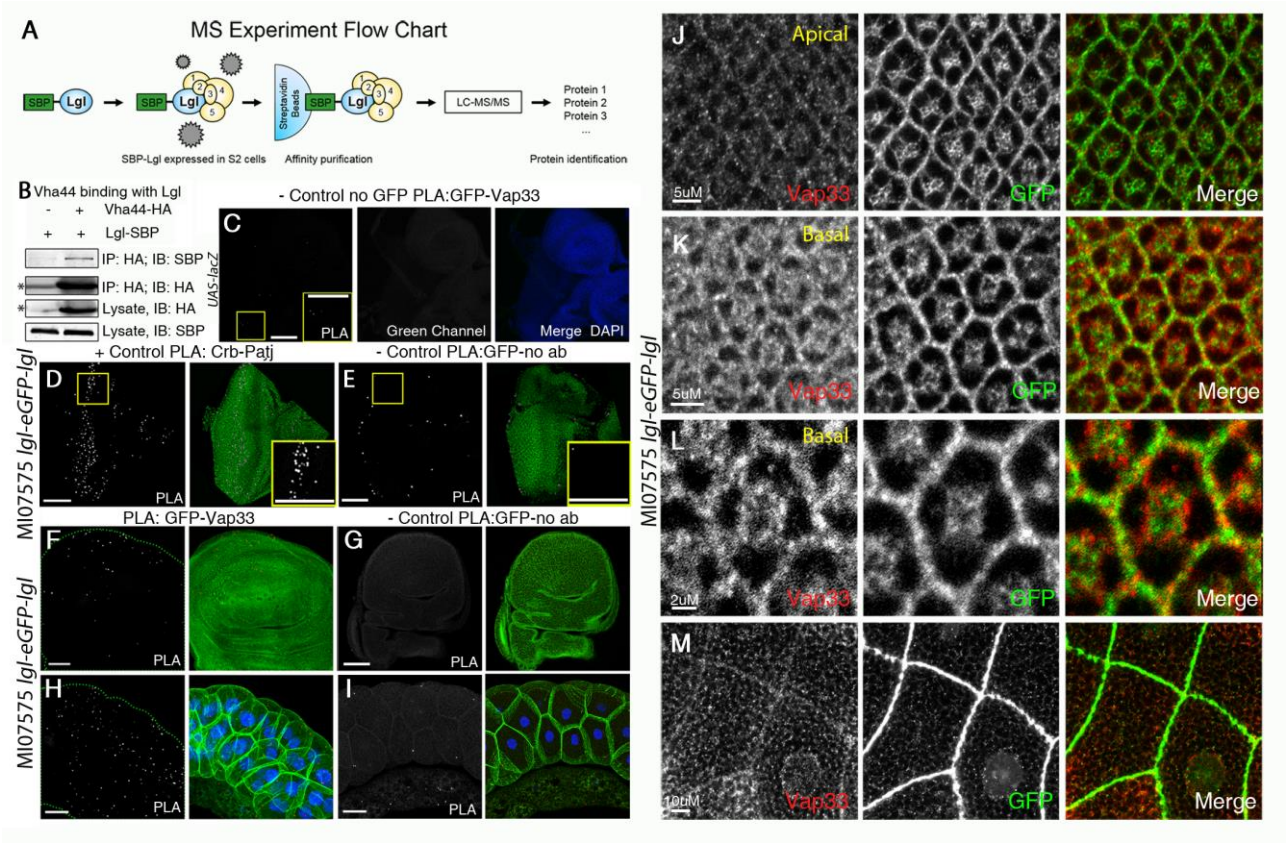

Fig. S2. Lgl physically interacts with Vap33 and the V-ATPase component Vha44.

(**A**) Mass Spectrometry experiment flow chart. (**B**) Coimmunoprecipitation of Vha44-HA and Lgl-SBP. Extracts from S2 cells co-expressing Lgl-SBP with or without Vha44-HA were immunprecipitated (IP) using an antibody specific for HA and immunoblotted for both SBP and HA. The asterisks indicate faint bands in the HA antibody lanes due to sample spill-over from the adjacent lane. N = 2 independent experiments. (**C**) Proximity ligation assay (PLA) negative control. Images show an eye disc without the GFP epitope (*UAS-lacZ*), stained with an antibody specific to GFP and an antibody specific to Vap33 for the PLA. The green channel shows that there is no GFP present. The merge panel also shows DAPI staining. (**D**) PLA positive control in *MI07575 lgl-eGFP-lgl* eye-antennal discs using an antibody specific for Crb and an antibody specific for Patj, showing foci throughout the tissue. (**E**) PLA negative control in *MI07575 lgl-eGFP-lgl* eye-antennal discs using only the primary antibody for GFP; no antibody to Vap33 was added. Nuclei are marked with DAPI. (**F–I**) In situ PLA in a *MI07575 lgl-eGFP-lgl* wing imaginal disc (F, G) and salivary gland (H, I) using an antibody specific to GFP (to detect Lgl) and an antibody specific to

Vap33. Endogenous Lgl is shown in green in the merges (F, H). Negative controls (no Vap33 antibody added) are shown in (G, I). Nuclei are stained with DAPI (blue). (**J–L**) Confocal planar images of *MI07575 lgl-eGFP-lgl* third instar larval eye imaginal discs (J, eye disc apical section; K, eye disc basal section; L, eye disc high magnification of basal section), and (**M**) a high magnification confocal image of a salivary gland, stained for Vap33 and Lgl-GFP. For (C-M), N = 3 independent experiments, n = 3 samples per genotype analysed for each experiment. Scale bars, 50 μm (C-I), 5 μm (J, K), 2 μm (L), or 10 μm (M).

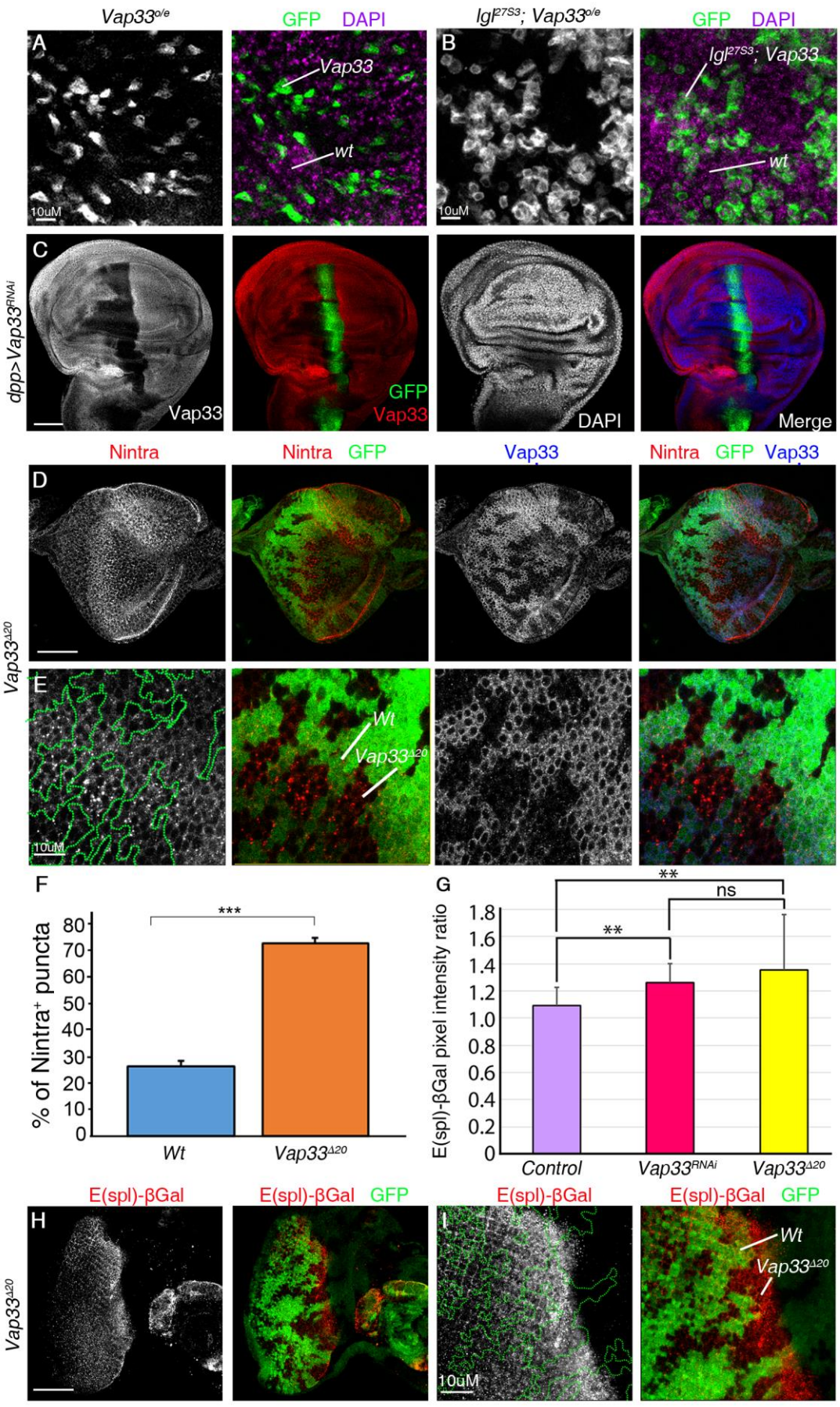
Vap33o/e
GFP DAPI
A
Vap33
wt
10uM
lgl27S3; Vap33o/e
GFP DAPI
B
lgl27S3; Vap33
wt
10uM
dpp>Vap33RNAi
C
Vap33
GFP
Vap33
DAPI
Merge
Vap33Δ20
Nintra
Nintra GFP
Vap33
Nintra GFP Vap33
D
E
Wt
Vap33Δ20
10uM
F
% of Nintra+ puncta
***
Wt
Vap33Δ20
G
E(spl)-βGal pixel intensity ratio
**
**
ns
Control
Vap33RNAi
Vap33Δ20
Vap33Δ20
E(spl)-βGal
E(spl)-βGal GFP
H
E(spl)-βGal
E(spl)-βGal GFP
I
Wt
Vap33Δ20
10uM

Fig. S3. Vap33-overexpressing tissue is retained in the pupal retina, and *Vap33* mutant tissue accumulates N-intra and increases expression of the Notch reporter.

(**A, B**) Confocal images of pupal retinas, showing that mutant tissue is retained. (A) $Vap33^{o/e}$ mosaic pupal eye disc at 52h after puparium formation (APF). $Vap33^{WT}$ clones are GFP-positive, and WT cells are GFP-negative. Nuclei are marked with DAPI (magenta). (B) lgl^{27S3} $Vap33^{o/e}$ mosaic pupal eye disc at 52h APF. lgl^{27S3} $Vap33^{WT}$ clones are GFP-positive, and WT cells are GFP-negative. Nuclei are marked with DAPI (magenta). (**C**) Confocal images of *dpp-GAL4* $Vap33^{RNAi}$ third instar larval wing discs stained for Vap33. Knockdown of *Vap33* using the *Vap33-RNAi* line reduced the amount of Vap33 protein in the *dpp* expression domain (green). Nuclei are stained with DAPI. For (**A-C**), N = 2 independent experiments, n = 3 samples analysed for each genotype per experiment. (**D–F**) Analysis of intracellular Notch protein localization as detected by staining with an antibody specific for the intracellular domain of Notch (N-intra) in $Vap33^{\Delta 20}$ mosaic third instar larval eye-antennal discs. (**D, E**) Confocal planar sections of $Vap33^{\Delta 20}$ mosaic eye-antennal epithelium stained for N-intra and Vap33. Mutant clones are GFP-negative. Low magnification (**D**) and high magnification (**E**) images from a region in the posterior part of the eye disc are shown. (**F**) Quantification of the number of N-intra–positive puncta in the mutant clones relative to the adjacent surrounding WT tissue. The graph represents the average percentage of N-intra–positive puncta in $Vap33^{\Delta 20}$ mutant clones relative to the surrounding WT tissue (P = 0.009). N = 3 independent experiments, n = 3-4 samples for each genotype analysed for each experiment. Error bars indicate S.E.M. *** P-value <0.0001 (T-tests with two tailed distribution and unequal variance). (**G–I**) Analysis of *E(spl)-lacZ* expression by staining for β-galactosidase (βGal) in $Vap33^{\Delta 20}$ mosaic third instar larval eye-antennal discs. (G) Quantification of pixel intensity ratio of βGal staining between WT cells and $Vap33^{\Delta 20}$ mutant clones. N = 3 independent experiments, n = 5 samples per genotype analysed for each experiment). Error bars indicate S.E.M. ** P-value=0.002: ns, differences not significant (T-tests with two tailed distribution and unequal or equal variance). (H, I) Confocal

planar sections of *Vap33*$^{\Delta 20}$ mosaic eye-antennal epithelium stained for βGal. Mutant clones are GFP-negative). Low magnification (H) and high magnification (I) images from a region in the posterior part of the eye disc are shown. *Vap33-RNAi* (from Fig. 3) is also shown for comparison. Scale bars, 10 μm (A, B, E) and 50 μm (C, D, H, I).

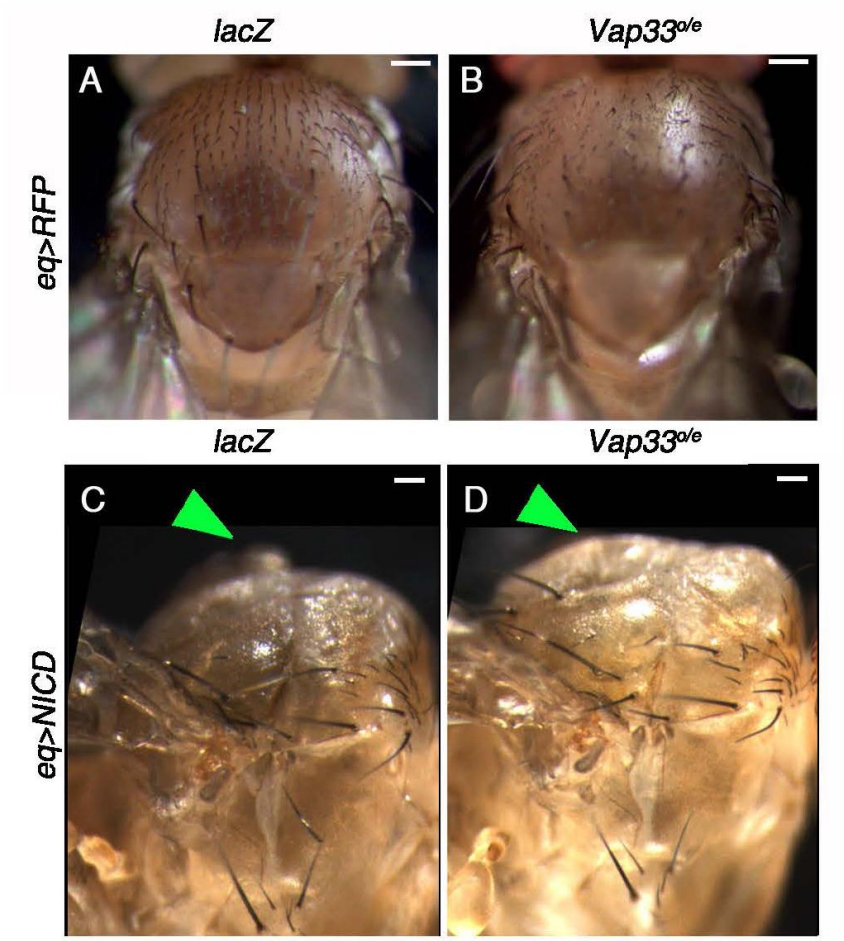

Fig. S4. Overexpression of Vap33 results in reduced bristle formation but does not suppress the NICD-induced thoracic overgrowth phenotype.

(**A, B**) Views of the dorsal surface of the adult thorax from control *eq>RFP* (A) and *eq>Vap33$^{o/e}$* (B). (**C, D**) Lateral views of the *eq>NICD* adult thorax phenotype and the genetic interaction with *Vap33$^{o/e}$*. Flies expressing *eq>NICD lacZ* (C), and flies expressing *eq>NICD Vap33$^{o/e}$* (D). Arrowheads indicate the *eq>NICD*–induced overgrown thorax. N = 2 independent experiments, n = 3 samples analysed for each genotype per experiment. Scale bars, 50 μm.

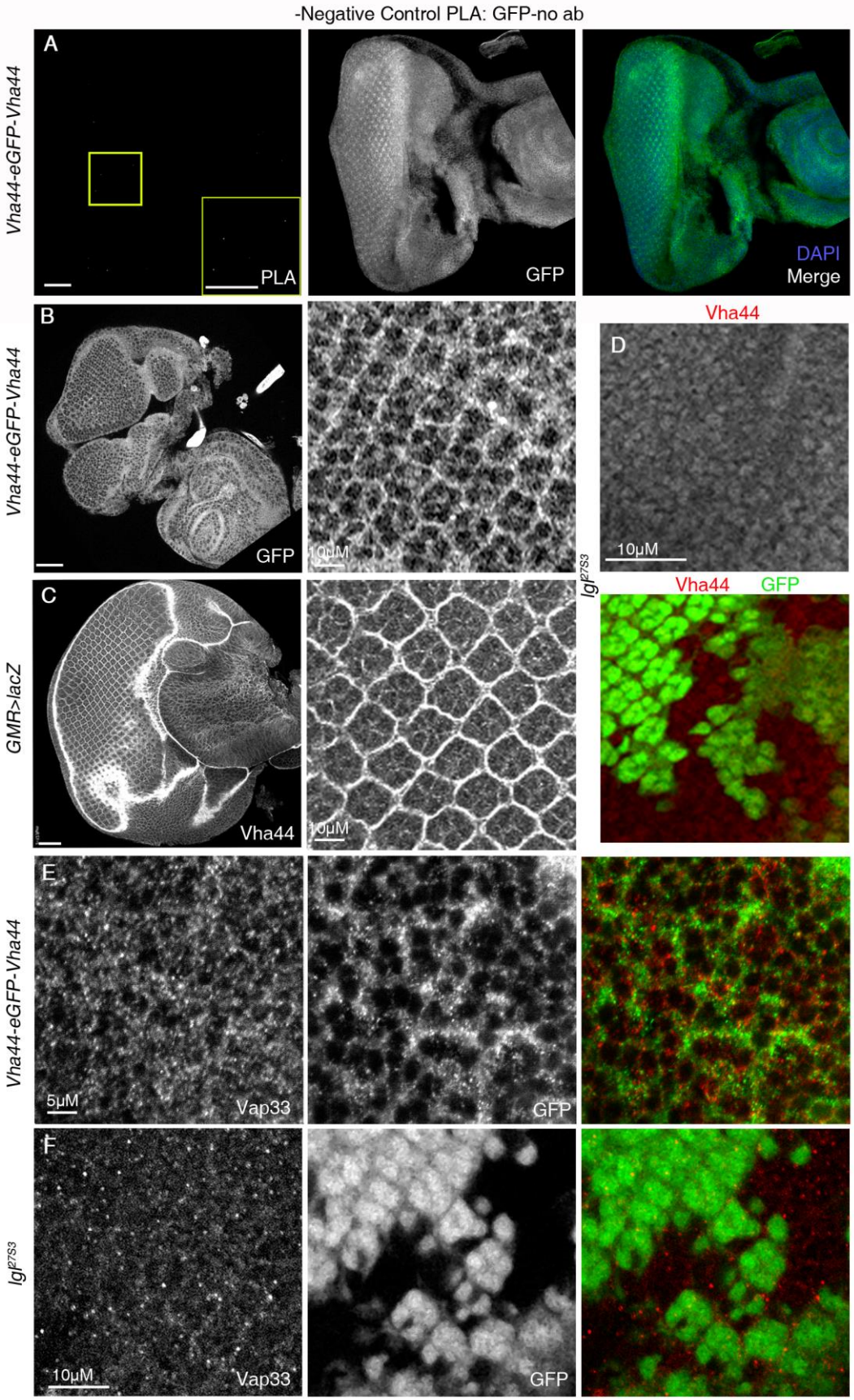
-Negative Control PLA: GFP-no ab
Vha44-eGFP-Vha44
A
PLA
GFP
DAPI
Merge
Vha44-eGFP-Vha44
B
GFP
10μM
Vha44
D
10μM
Igl2753
GMR>lacZ
C
Vha44
10μM
Vha44
GFP
Vha44-eGFP-Vha44
E
5μM
Vap33
GFP
Igl2753
F
10μM
Vap33
GFP

Fig. S5. Vap33 colocalizes with Vha44-GFP, and Vap33 protein abundance and localization are unaffected in *lgl* mutant tissue.

(**A**) Confocal planar images of the control proximity ligation assay (PLA) in *MI11080 Vha44-eGFP-Vha44* eye discs using only the antibody specific for GFP with no antibody specific for Vap33 added. (**B**) Confocal planar images of third instar larval *MI11080 Vha44-eGFP-Vha44* eye disc stained for GFP showing localization of the Vha44-GFP protein at low or high magnification. (**C**) A control, *GMR>lacZ*, eye disc stained for Vha44 and shown at low or high magnification. (**D**) lgl^{27S3} mosaic eye discs stained for Vha44. lgl^{27S3} mutant tissue is GFP-negative. (**E, F**) Confocal images of *MI11080 Vha44-eGFP-Vha44* eye discs stained for Vap33 and Vha44-GFP (E) and lgl^{27S3} mosaic eye discs (*lgl* mutant tissue is GFP-negative) stained for Vap33 (F). N = 2 independent experiments, n = 3 samples analysed for each genotype per experiment. Scale bars, 50 μm (A-C), 10 μm (D, F), and 5 μm (E).

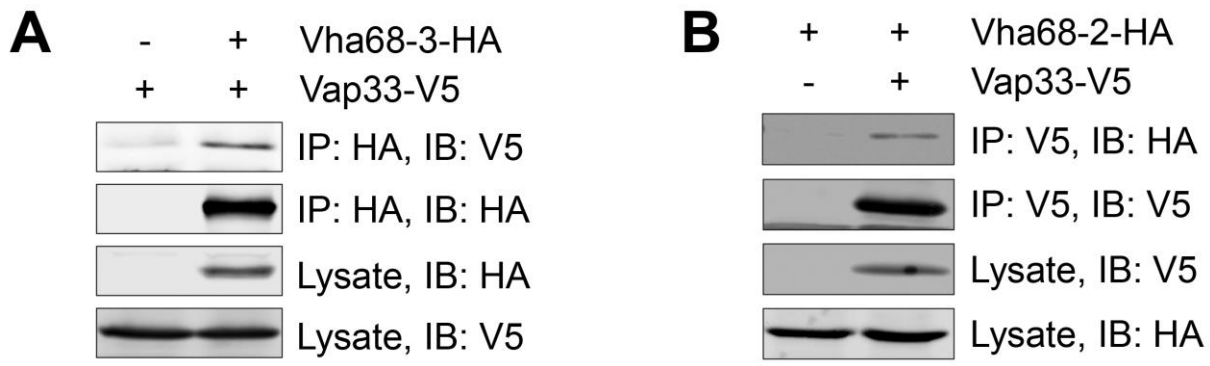

Fig. S6. Vap33 physically interacts with Vha68-3 and Vha68-2.

(**A**) Immunoblot showing the co-immunoprecipitation of Vap33 and Vha68-3 from S2 cells expressing Vap33-V5 alone or coexpressing Vap33-V5 and Vha68-3-HA, when the experiment was conducted in the reverse manner as that shown in Fig. 7. Vha68-3-HA was immunoprecipitated (IP) with an antibody specific for HA from extracts from S2 cells expressing Vap33-V5 or coexpressing Vap33-V5 and Vha68-3-HA, and immunoblotted (IB) with an antibody specific for V5. (**B**) Immunoblot showing the co-immunoprecipitation of Vha68-2-HA with Vap33-V5 from S2 cells expressing Vha68-2-HA alone or coexpressing Vha68-2-HA and Vap33-V5. These experiments were conducted once (N=1).

Table S1. *Drosophila* stocks and references.

***Drosophila* stock**	**Source and reference**
l(2)gl^{27S3} (denoted as *lgl^{27S3}*)	(34)
P(E(spl)m8-HLH-2.61)2 (denoted as *E(spl)lacZ$^{m8\text{-}2.61}$* or *E(spl)lacZ,*)	A. Bergmann (56) on chromosome *2R* (57)
P(GAL4-Hsp70.PB)l(3)Eq1^{Eq1} (denoted as *Eq1-GAL4* or *eq>*)	H. Sun (79)
P(w[+mC]=UAS-NEXT.HA) (denoted as *UAS-NEXT, (III))*	T. Vaccari (78)
P(UAS-N.icd) (denoted as *UAS-NICD (II)*	S. Artavanis-Tsakonas (81)
P(UAS-lacZ.nls) (denoted as *UAS-lacZ-nls (III))*	G. Baeg
P(UAS-Vha44.P) (denoted as *UAS-Vha44*)	M. Simons (84)
Vap33$^{\Delta 20}$ (Loss-of-function allele, generated by imprecise excision of *P(lArB)* of *Vap-33-1^{47}*)	H. Bellen ((90)
w^{1118} (denoted as *w*) - Used as *wild-type* control.	BL3605, Bloomington Stock Center
P(GAL4-GMR) (denoted as *GMR-GAL4*)	B. Hay (77)
P(UAS-mam.DN) (denoted as *UAS-mam^{DN}*)	BL26672, Bloomington Stock Center ((82)
Vha68-2^{R6} (EMS generated null mutant, due to stop codon mutation)	BL39621, Bloomington Stock Center ((51)
P(UAS-myr-mRFP)2 (denoted as *UAS-myr-mRFP*)	BL7119, Bloomington stock Center
P(y[+t7.7] w[+mC]=10XUAS-mCD8::GFP)attP2 (denoted as *UAS-CD8-GFP,*)	BL32184, Bloomington stock Center
Mi(y[+mDint2]=MIC)l(2)gl[MI07575] (denoted as *MI07575 lgl-eGFP-lgl*	BL43734, Bloomington stock Center (74)
P(w[+mC]=UAS-FLAG.Vap-33-1.HA)2 (denoted as *UAS-Vap33-HA*,	BL39682, Bloomington stock Center (76)
P(w[+mC]=UAS-Vap-33-1.P)3 (denoted as *UAS-Vap33*)	BL26693, Bloomington stock Center (8)
Mi(y[+mDint2]=MIC)Vha44[MI11080]/SM6a (denoted as *MI11080 Vha44-eGFP-Vha44*	BL56118, Bloomington stock Center (74)
P(w[+mW.hs]=GAL4-dpp.blk1)40C.6 (denoted as *dpp^{blk}-GAL4*)	BL1553, Bloomington stock Center
P(TRiP.JF01355)attP2 (denoted as *UAS-luciferase^{RNAi}*)	BL31603, Bloomington stock Center
P(GD3990)v30404 (denoted as *UAS-Vap33^{RNAi}*, v30404)	Vienna *Drosophila* Resource Center (119)
P(GD9363)v46554 (denoted as *UAS-Vha55^{RNAi}*, v46553)	Vienna *Drosophila* Resource Center (119)
P(ry[+t7.2]=neoFRT)19A (denoted as *FRT19A*)	BL1709, Bloomington stock Center
P(ey3.5-FLP.B)1, y^{1} w*; P(w(+mC)=UAS-mCD8::GFP.L)Ptp4E(LL4); P(w(+mC)=tubP-GAL80)LL10 P(ry(+t7.2)=neoFRT)40A; P(w(+mC)=tubP-GAL4)LL7 (denoted as *ey-FLP, UAS-GFP; Tub-GAL80, FRT40A;*	(33)

Tub-GAL4/TM6B (*ey-FLP MARCM 2L*)).	
P(ey3.5-FLP.B)1, y^1 w^* ; P(Ubi-GFP.nls)2L P(ry[+t7.2]=neoFRT)40A (denoted as *ey-FLP; FRT40A, Ubi-GFP*)).	A. Bergmann
y[1] w[*]; Pvr[1] P(ry[+t7.2]=neoFRT)40A (denoted as *FRT40A*).	BL58427, Bloomington stock Center
w^{1118} P{ry[+t7.2]=ey-FLP.N}2; P{w[+mC]=GMR-myr-mRFP}2L P{ry[+t7.2]=neoFRT}40A/CyO (denoted as *eyFLP, GMR-RFP FRT40A)*	BL7122, Bloomington Stock Center

Table S2. List of genotypes of the samples used in each figure.

Figure 1	**Genotype**
(A, B)	*eyFLP; FRT40A, E(spl)m8-lacZ / Ubi-GFP, FRT40A*
(C, D)	*eyFLP; lgl^{27S3}, FRT40A, E(spl)m8-lacZ /Ubi-GFP, FRT40A*
(E, F)	*eyFLP; lgl^{27S3}, Vha68.2^{R6}, FRT40A, E(spl)m8-lacZ /Ubi-GFP, FRT40A*
(I-K)	*eyFLP; lgl^{27S3}, FRT40A, E(spl)m8-lacZ /Ubi-GFP, FRT40A*
Figure S1	
(A-C)	*eyFLP; Vha68-2^{R6}, FRT40A, E(spl)m8-lacZ/Ubi-GFP, FRT40A*
(D)	*eyFLP; lgl^{27S3}, Vha68.2^{R6}, FRT40A, E(spl)m8-lacZ /Ubi-GFP, FRT40A*
Figure 2	
(C)	*y,w; MiMIC lgl MI07575*
(D)	*w/y, w; GMR-GAL4/+ ; UAS-FLAG.Vap33-HA*
Figure S2	
(C)	*w; UAS-lacZ*
(D-M)	*y,w; MiMIC lgl MI07575*
Figure 3	
(A, B)	*eyFLP; FRT40A, E(spl)m8-lacZ / Ubi-GFP, FRT40A*
(C, D)	*eyFLP; lgl^{27S3}, FRT40A, E(spl)m8-lacZ / Ubi-GFP, FRT40A*
(E, F)	*w, eyFLP, UAS-GFP; lgl^{27S3}, FRT40A, E(spl)m8-lacZ; UAS-Vap33$^{o/e}$ /Tub-GAL80, FRT40A, Tub-GAL4*
(G, H)	*w, eyFLP, UAS-GFP; FRT40A, E(spl)m8-lacZ; UAS-Vap33$^{o/e}$ / Tub-GAL80, FRT40A, Tub-GAL4*
(I, J)	*w, eyFLP, UAS-GFP; FRT40A, E(spl)m8-lacZ ; UAS-Vap33^{RNAi}/Tub-GAL80, FRT40A, Tub-GAL4*
(K, L)	*w, eyFLP, UAS-GFP; lgl^{27S3}, FRT40A, E(spl)m8-lacZ ; UAS-Vap33^{RNAi}*

	/ Tub-GAL80, FRT40A, Tub-GAL4
Figure S3	
(A)	*w, eyFLP, UAS-GFP; FRT40A, E(spl)m8-lacZ ; UAS-Vap33$^{o/e}$ /Tub-GAL80, FRT40A, Tub-GAL4*
(B)	*w, eyFLP, UAS-GFP; lgl^{27S3} , FRT40, E(spl)m8-lacZ ; UAS-Vap33$^{o/e}$ / Tub-GAL80, FRT40A, Tub-GAL4*
(C)	*UAS-mCD8-GFP; dpp-GAL4 / UAS-Vap33^{RNAi}*
(D-E, H-I)	*Vap33$^{\Delta 20}$, FRT19A/ Ubi-GFP, FRT19A; eyFLP/+*
Figure 4	
(A)	*w;; UAS-myrRFP, Eq1-GAL4/UAS-lacZ*
(B)	*w;; UAS-myrRFP, Eq1-GAL4/ UAS-Vap33^{RNAi}*
(C)	*w;; UAS-myrRFP, Eq1-GAL4/ UAS-Vap33$^{o/e}$*
(D)	*w;; UAS-myrRFP, Eq1-GAL4/ UAS-Vha55^{RNAi}*
(E)	*w;; UAS-myrRFP, Eq1-GAL4/ UAS-Vha44$^{o/e}$*
(F)	*w;; UAS-myrRFP, Eq1-GAL4, UAS-NEXT/UAS-lacZ*
(G)	*w;; UAS-myrRFP, Eq1-GAL4, UAS-NEXT/UAS-Vap33^{RNAi}*
(H)	*w;; UAS-myrRFP, Eq1-GAL4, UAS-NEXT/ UAS-Vap33$^{o/e}$*
(I)	*w;; UAS-myrRFP, Eq1-GAL4, UAS-NEXT/UAS-Vha55^{RNAi}*
(J)	*w;; UAS-myrRFP, Eq1-GAL4, UAS-NEXT/UAS-mam^{DN}*
Figure S4	
(A, C)	*w; UAS-NICD; UAS-myrRFP, Eq1-GAL4 / UAS-lacZ*
(B, D)	*w; UAS-NICD; UAS-myrRFP, Eq1-GAL4 /UAS-Vap33$^{o/e}$*
Figure 5	
(A)	*eyFLP; FRT40A, E(spl)m8-lacZ /Ubi-GFP, FRT40A*
(B)	*Vap33$^{\Delta 20}$, FRT19A/ Ubi-GFP, FRT19A; eyFLP/+*

(C)	*eyFLP; lgl^{27S3}, FRT40A, E(spl)m8-lacZ /Ubi-GFP, FRT40A*
(D)	*w, eyFLP, UAS-GFP; lgl^{27S3}, FRT40A, E(spl)m8-lacZ; UAS-Vap33$^{o/e}$ / Tub-GAL80, FRT40A, Tub-GAL4*
(E)	*w, eyFLP, UAS-GFP; FRT40A, E(spl)m8-lacZ; UAS-Vap33$^{o/e}$/ Tub-GAL80, FRT40A, Tub-GAL4*
Figure 6	
(A)	*y, w; MiMIC Vha44 MI11080*
(B)	*w; GMR-GAL4; UAS-luciferase^{RNAi}*
(C)	*w; GMR-GAL4; UAS-luciferase^{RNAi}/ UAS-Vap33^{WT}*
(D)	*w; GMR-GAL4; UAS-luciferase^{RNAi}/ UAS-Vha44*
(E)	*w; GMR-GAL4; UAS-Vap33^{WT}/ UAS-Vha44*
(G)	*w; GMR-GAL4; UAS-lacZ*
(H)	*w; GMR-GAL4; UAS-lacZ/ UAS-Vap33$^{o/e}$*
(I)	*w; GMR-GAL4; UAS-lacZ/ UAS-Vha44$^{o/e}$*
(J)	*w; GMR-GAL4; UAS-Vap33$^{o/e}$/ UAS-Vha44 $^{o/e}$*
Figure S5	
(A, B, E)	*y, w; MiMIC Vha44 MI11080*
(C)	*w; GMR-GAL4; UAS-lacZ*
(D, F)	*eyFLP; lgl^{27S3}, FRT40A, E(spl)m8-lacZ/Ubi-GFP, FRT40A*
Figure 7	
(D)	*eyFLP; lgl^{27S3}, FRT40A, MiMIC Vha44 MI11080/GMR-myrRFP, FRT40A*

Data file S1. Lgl-interacting proteins.

This list is provided in a separate Excel file. A ranked list of Lgl interacting proteins identified in stable S2 cells, based on their AvgP scores determined by SAINT analysis, relative to 6 control samples (biological replicates using untransfected S2 cells). AP-MS of Lgl-interacting proteins was performed in two independent biological replicates (LGL, LGL2). Individual columns in the table are the following. Bait: the name of the bait protein (Lgl); Prey: FlyBase gene identifier for the identified interactor; PreyGene: common gene name for the identified interactor; IP: two experimental samples, LGL and LGL2; Spec: the number of peptides identified for the interacting protein in two experiments (LGL and LGL2), separated by a vertical line; SpecSum: the sum of peptide values from column Spec; NumRep: number of experimental repetitions (2); iProb: individual probability of interaction based on each experimental sample; ctrlCounts: numbers of peptides identified for the interactor (Prey) protein in 6 control samples, separated by vertical lines; AvgP: average probability of interaction (main sorting parameter) calculated as an average of probabilities in the iProb column; MaxP: maximum interaction probability value from the iProb column.